CALPHAD: Computer Coupling of Phase Diagrams and Thermochemistry 70 (2020) 101791

Contents lists available at ScienceDirect

Calphad

journal homepage: http://www.elsevier.com/locate/calphad

Second nearest-neighbor modified embedded-atom method interatomic potentials for the Co-M (M = Ti, V) binary systems

Sang-Ho Oh, Donghyuk Seol, Byeong-Joo Lee *

Department of Materials Science and Engineering, Pohang University of Science and Technology (POSTECH), Pohang, 37673, Republic of Korea

ARTICLE INFO

Keywords:
2NN MEAM
Interatomic potential
Co–Ti
Co–V
Nano catalyst

ABSTRACT

Interatomic potentials for the Co–Ti and Co–V binary alloy systems have been developed based on the second nearest-neighbor modified embedded-atom method (2NN MEAM) interatomic potential formalism. Newly developed potentials reproduce various structural and thermodynamic properties of the binary alloys in reasonable agreement with experiments, first-principles calculations, and CALPHAD-type thermodynamic assessments. It is emphasized that these potentials can serve as groundwork for atomistic studies on the design of highly efficient trimetallic noble metal catalysts.

1. Introduction

Noble metal nano-catalysts, especially palladium (Pd) and platinum (Pt), have received attention for their various applications and long lifespan during the reaction. Further, adding other alloying elements to a pure noble metal has been suggested as a means to reduce the expense and increase catalytic properties [1,2]. Among the alloying elements, cobalt is recommended to achieve better catalytic properties [3–7]. Further improvements can be achieved by adding a third element such as iron (Fe), nickel (Ni), vanadium (V), or titanium (Ti), which improves the catalytic properties of the noble metal [3].

To examine catalytic properties, investigating the shape and the atomistic configuration of the nanoparticles is necessary. However, precise control and analysis of these factors are quite difficult due to the high sensitivity of nanoscale structures to experimental conditions [8]. To overcome experimental limits and explore new alloying elements, atomistic simulations are a useful approach.

Although the most accurate atomistic simulation method to estimate solid state materials properties may be the first-principles calculations, it is not suitable for large-scale atomistic simulations such as the case of nanoparticles containing thousands of atoms. In this case, semi-empirical atomistic simulations such as molecular dynamics (MD) and Monte Carlo (MC) based on interatomic potentials can be a powerful method, reasonably predicting the properties of nanoparticles such as the surface chemistry, shape evolution, or the composition [9]. In the present work, second nearest-neighbor modified embedded-atom method (2NN MEAM) formalism was chosen due to its capability of describing various structures including FCC, BCC, and HCP and the relatively low limit on the number of atoms compared to the first-principles method [10].

In the 2NN MEAM formalism, interatomic potentials for unary systems including Pt and Pd [11], and several binary alloy systems that include Pt [9] and Pd [12] are already available. However, no interatomic potential for ternary systems has been developed yet. To develop an interatomic potential for a ternary system, three unary parameter sets and three binary sets are needed. In case of the probable elements mentioned above, interatomic potentials for Co-Fe [13] and Co–Ni [14] binary systems are already published, but no potential for Co–Ti and Co–V systems has been developed. In the present work, the Co–Ti and Co–V binary interatomic potentials were newly developed within the 2NN MEAM formalism as a prior work for the development of Pt–Co-M and Pd–Co-M ternary interatomic potentials and atomistic simulations for the design of trimetallic nano-catalysts.

2. Determination of interatomic potential parameters

The development of the 2NN MEAM interatomic potential for a binary system is based on potentials for constituent unary systems. Interatomic potentials for pure Co [15], Ti [16], and V [17] already developed are listed in Table 1.

To describe a binary system using the 2NN MEAM, a reference structure and 14 independent parameters have to be determined: cohesive energy (E_c), equilibrium distance (R_e), bulk modulus (B), d^+ and d^-, 8 screening factors (C_{min} and C_{max}), and the ratio between

* Corresponding author.
E-mail address: calphad@postech.ac.kr (B.-J. Lee).

https://doi.org/10.1016/j.calphad.2020.101791
Received 19 December 2019; Received in revised form 3 May 2020; Accepted 23 May 2020
Available online 15 June 2020

Table 1
2NN MEAM potential parameter sets for pure Co [15], Ti [16], and V [17]. The units of the cohesive energy E_c, equilibrium nearest-neighbor distance r_e, and bulk modulus B are eV, Å, and 10^{12} dyne/cm^2, respectively. The reference structure is bcc for V and hcp for Co and Ti.

	E_c	r_e	B	A	$\beta^{(0)}$	$\beta^{(1)}$	$\beta^{(2)}$	$\beta^{(3)}$	$t^{(1)}$	$t^{(2)}$	$t^{(3)}$	C_{min}	C_{max}	d
Co	4.41	2.500	1.948	0.9	3.50	0.0	0.0	4.0	3.50	5.00	−1.00	0.49	2.00	0.00
Ti	4.87	2.920	1.097	0.66	2.70	1.0	3.0	1.0	6.80	−2.00	−12.0	1.00	1.44	0.00
V	5.30	2.625	1.570	0.73	4.74	1.0	2.5	1.0	3.30	3.20	−2.00	0.49	2.80	0.00

Table 2
2NN MEAM potential parameter sets for the Co–Ti and Co–V binary systems. The units of the cohesive energy E_c, equilibrium nearest-neighbor distance r_e, and bulk modulus B are eV, Å, and 10^{12} dyne/cm^2, respectively.

	Co–Ti	Co–V
Reference	B2-type CoTi	$L1_2$-type Co_3V
E_c	$0.5E_c^{Co}+0.5E_c^{Ti}+0.4280$	$0.75E_c^{Co}+0.25E_c^{V}+0.1400$
r_e	2.530	2.511
B	1.763	1.853 ($0.75\ B^{Co}+ 0.25\ B^{V}$)
C_{min} (Co-M-Co)	0.49 (C_{min}^{Co})	0.14
C_{min} (M-Co-M)	1.00 (C_{min}^{Ti})	1.20
C_{min} (Co–Co-M)	0.49	0.20
C_{min} (Co-M-M)	0.72	0.49
C_{max} (Co-M-Co)	2.00 (C_{max}^{Co})	2.80
C_{max} (M-Co-M)	2.80	2.80 (C_{max}^{V})
C_{max} (Co–Co-M)	1.44	1.96
C_{max} (Co-M-M)	2.80	2.80
d	0.00	0.00
$\rho_0^A:\rho_0^B$	1:1	1:1

atomic electron density scaling factors (ρ_0^A/ρ_0^B). The reference structure is a perfectly-ordered intermetallic compound in which all atoms have the same type of atoms as the second nearest-neighbors. In the present work, B2 CoTi and $L1_2$ Co_3V compounds were selected as reference structures for the Co–Ti and Co–V systems, respectively. E_c and R_e parameters were determined by fitting the cohesive energy and the lattice parameter of existing phases in the phase diagram. Elastic moduli were also considered for the determination of B parameters. d and ρ_0^A/ρ_0^B parameters were given the average values of constituent pure elements of the system. Screening factors were determined by fitting known fundamental material properties from experiments, first-principles calculations, and CALPHAD-type thermodynamic assessments [21,22,24–42]. Finally determined potential parameter sets are listed in Table 2. Details of the 2NN MEAM formalism are given in the Supplementary Information.

2.1. Calculation of fundamental material properties

The reliability of the newly developed potentials was checked by comparing the calculated fundamental materials properties with experimental data, first-principles calculations, and CALPHAD

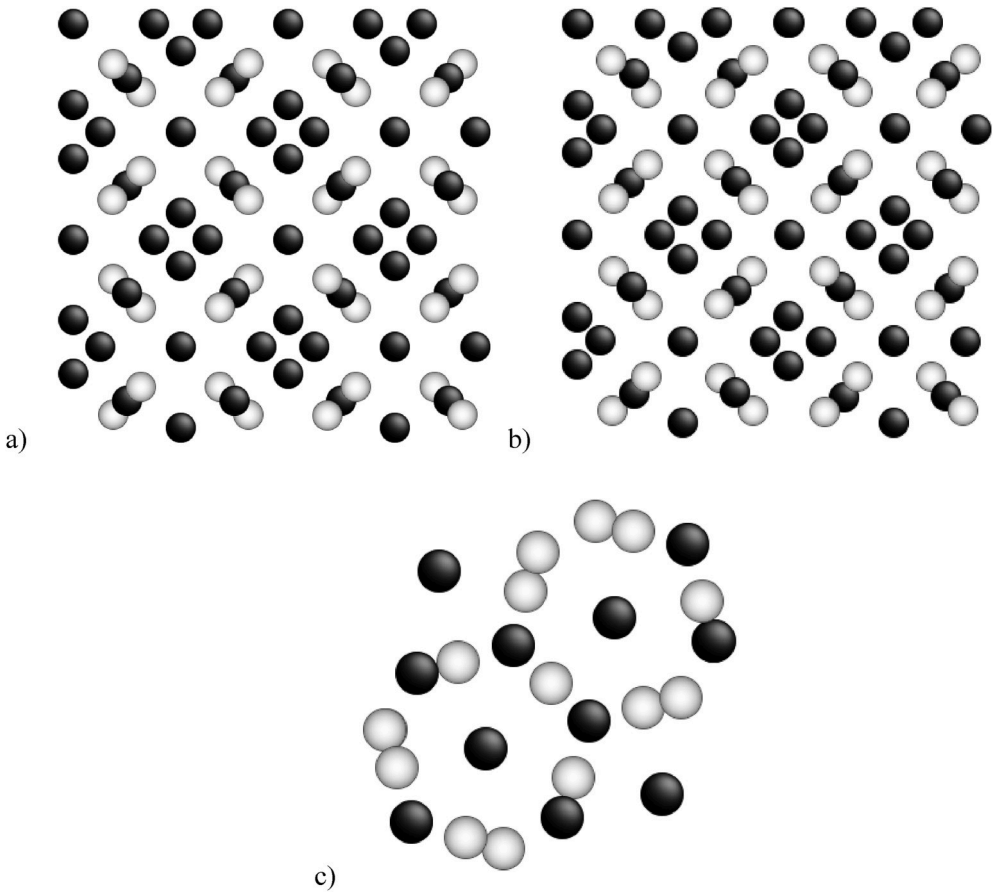

Fig. 1. Unit cell of a) original $E9_3$ $CoTi_2$, b) locally relaxed $E9_3$ $CoTi_2$, and c) $D8_b$ CoV sigma phase, used in the present work. White atoms are for cobalt, black for titanium and vanadium.

Table 3
Calculated lattice constants (Å) of Co_xTi_y and Co_xV_y intermetallic compounds at 0 K using the present 2NN MEAM potential, in comparison with experimental data and other calculations.

Compound	Structure	Present work	Expt.	First-Principles
$CoTi_2$	cF96 ($E9_3$)	11.09	11.283 [24]	
			11.29 [25]	
CoTi	cP2 (B2)	2.92	2.988 [24]	
			2.995 [26]	
Co_2Ti	cF24 (C15)	6.63	6.691 [27]	
			6.706 [28]	
	hP24 (C36)	(a) 4.70	4.72 [24]	
		(c) 15.25	15.392 [24]	
Co_3Ti	cP4 ($L1_2$)	3.61	3.602 [26]	3.601 [29]
			3.614 [26]	3.588 [30]
CoV_3	cP8 (A15)	4.69	4.691 [31]	4.671 [32]
$Co_{0.4}V_{0.6}$	tP30 ($D8_b$)	(a) 8.92	8.843–9.032 [33]	
		(c) 4.65	4.586–4.661 [33]	
Co_3V	cP4 ($L1_2$)	3.55		3.514 [29]
				3.51 [34]
	hP24	(a) 5.03	5.032 [35]	4.997 [34]
		(c) 12.28	12.30 [35]	12.01 [34]

assessments. Comparisons of lattice constant, elastic moduli, enthalpy of formation, and enthalpy of mixing for compounds and solution phases assure the quality of fitting and the reasonability of newly developed potentials. KISSMD, an in-house molecular dynamics (MD) and statics (MS) code, and the Large-scale Atomic/Molecular Massively Parallel Simulator (LAMMPS) package were used for the MD calculation. Most of the calculations were performed at 0 K, except for the calculation of the enthalpy of mixing for liquid alloys and structural stability at finite temperatures. A periodic boundary condition was set in all directions, and the radial cutoff distance was 4.8 Å – sufficiently larger than the second nearest-neighbor distances in pure Co, Ti, and V unary systems.

The Co–Ti binary phase diagram [18] shows several compounds such as $E9_3$ $CoTi_2$, B2 CoTi, C15 and C36 Co_2Ti, and $L1_2$ Co_3Ti. Meanwhile, the Co–V binary phase diagram [20] shows hP24 and $L1_2$ Co_3V, $D8_b$ CoV, and A15 CoV_3. In the case of the $D8_b$ CoV phase, each element prefers different sites, and the most stable structure was used in the present work. In addition, the stability of $L1_2$ Co_3V phase has been controversial, and recently it was concluded as a metastable phase [20,49,50]. Despite of the controversy, $L1_2$ phase was also examined in the present work to enrich fitting references. The $CoTi_2$ sample, which shows a slight local relaxation of atoms compared to the original version [19], and the CoV sample with the most stable atomic arrangement are presented in Fig. 1.

The calculated lattice constants of compounds are compared with experimental data and first-principles calculations in Table 3. The calculated lattice constants of the Co-rich FCC random solid solution phases and the $D8_b$ CoV sigma phase are presented along the composition in Fig. 2, in comparison with experimental data. The calculated elastic moduli of the reference structures are also compared with data from the literature in Table 4. Although the calculated elastic moduli of $L1_2$ Co_3V are somewhat smaller than a first-principles calculation, it was unavoidable to reproduce the thermodynamic stability of other phases.

To examine the reliability of the potentials in thermodynamic properties, the enthalpy of formation of stable and hypothetical metastable phases for each binary system was calculated, as presented in Fig. 3 and in Table 5, in comparison with experimental data, first-principles calculations, and thermodynamic assessments. The drawn convex hulls are based on the prediction from the developed interatomic potentials. Ideally, the convex hull curve should consist of the enthalpy value of only stable phases, and metastable phases should not have enthalpy of formation value below the hull. Although few mismatches exist, they can be rationalized as described below and can be finally accepted.

In the case of the Co–Ti binary system, the enthalpy of formation for the $E9_3$ $CoTi_2$, and B2 CoTi compounds are reproduced in good

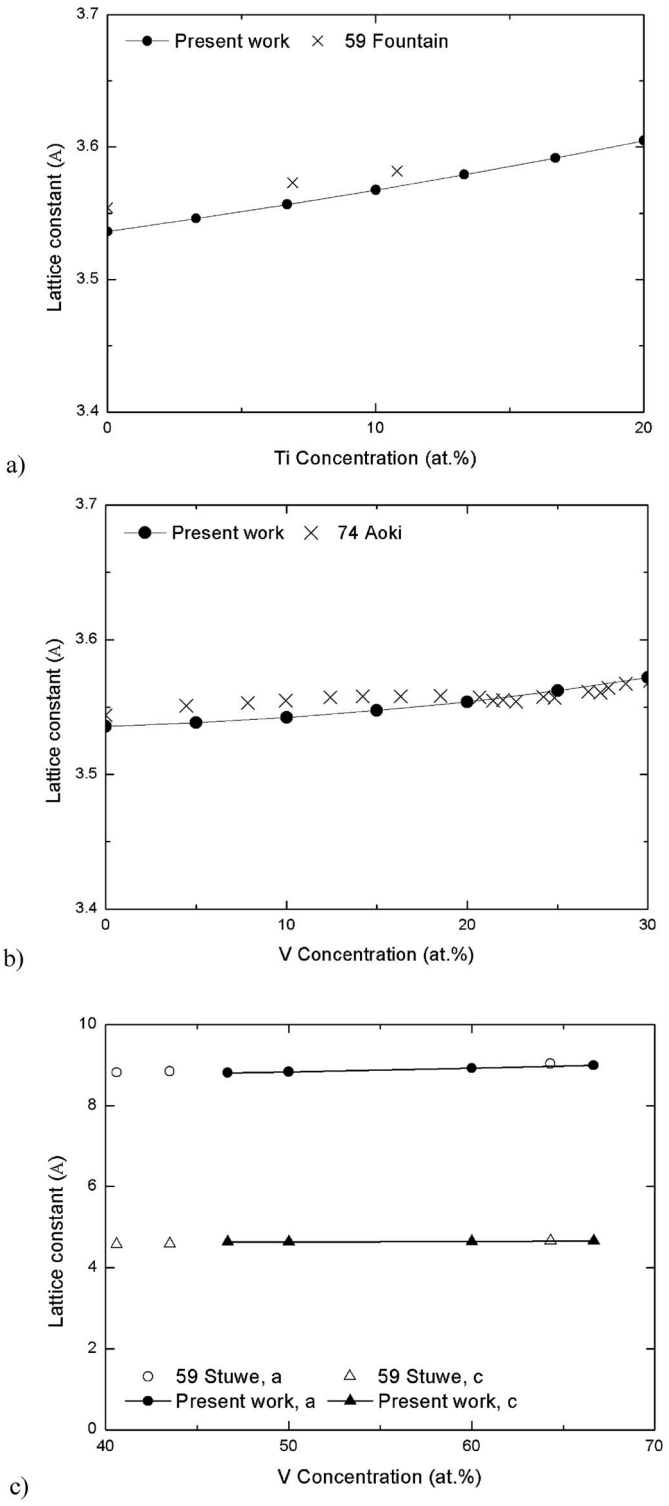

Fig. 2. Lattice constant of Co-rich a) fcc solid solution of Co-Ti and b) Co-V binary systems, and c) $D8_b$ CoV sigma phase at 0 K according to the present interatomic potential, in comparison with experimental data [26,33,43].

agreement with first-principles calculation [21] and an experiment [22] (see Table 5), and they are the most stable phase among the possible compounds at corresponding compositions (see Fig. 3a). Meanwhile, the hypothetical $D0_{19}$ Co_3Ti phase is calculated to be slightly more stable than the $L1_2$ Co_3Ti, and the hypothetical C14 Co_2Ti phase has a slightly lower enthalpy of formation value than the C36 and C15 phases. A first-principles calculation also shows that C14 can be more stable at 0 K

Table 4
Calculated elastic moduli (GPa) of reference structures at 0 K using the present 2NN MEAM potential, in comparison with experimental data and other calculations.

Compound	Structure		Present work	Expt.	First-Principles
CoTi	cP2 (B2)	B	176.25	154 [36]	188.6 [37]
		C11	299.05	203 [36]	
		C12	114.85	129 [36]	
		C44	125.15	68 [36]	
Co_3V	cP4 ($L1_2$)	B	185.29		255.447 [29]
		C11	260.37		392.739 [29]
		C12	147.75		186.802 [29]
		C44	80.20		190.327 [29]

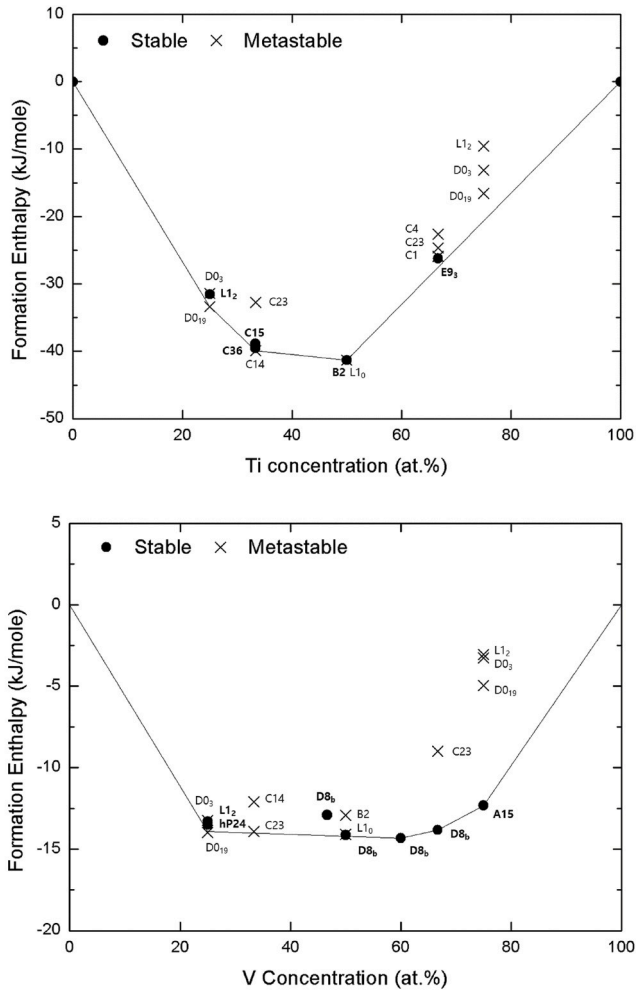

Fig. 3. Enthalpy of formation of stable and hypothetical metastable phases of the a) Co-Ti and b) Co-V binary systems at 0 K according to the present interatomic potentials.

than C15 [21]. It should be noted here that the $D0_{19}$ structure has the same symmetry and stacking sequence as pure cobalt and titanium, and the C14 has a layer sequence more similar to cobalt and titanium than the C15 and C36 (C14 has a 'XY' sequence, while C15 and C36 have 'XYZ', and 'XYZY' sequences, respectively [23]). In addition, the $L1_2$ and C36 phases have a composition range on the phase diagram, which indicates a high possibility of the existence of defects. Therefore, it is not surprising to see that the metastable $D0_{19}$ and C14 phases are calculated to be slightly more stable (by less than 0.04 eV) than the other stoichiometric equilibrium phases at 0 K.

In the case of the Co–V system, A15 CoV_3 and $D8_b$ CoV sigma phases

Table 5
Calculated enthalpy of formation (kJ/mole) of Co_xTi_y, Co_xV_y intermetallic compounds at 0 K using the present 2NN MEAM potential, in comparison with experiments and other calculations.

Compound	Structure	Present work	Expt.	First-Principles	CALPHAD
$CoTi_2$	cF96 ($E9_3$)	−26.2	−33.0 [38]	−27.57 [21]	−33.763 [39]
CoTi	cP2 (B2)	−41.3	−41.3 [22]	−37.28 [21]	−42.177 [39]
			−44.3 [40]		
Co_2Ti	cF24 (C15)	−38.9		−29.04 [21]	−28.219 [39]
	hP24 (C36)	−39.4	−34.1 [40]		−27.246 [39]
	[a] hP12 (C14)	−39.9		−30.05 [21]	
Co_3Ti	cP4 ($L1_2$)	−31.6		−24.58 [21]	−20.823 [39]
				−25.843 [29]	
	[a] hP8 ($D0_{19}$)	−35.0		−24.759 [29]	
CoV_3	cP8 (A15)	−12.3			
$Co_{40}V_{60}$	tP30 ($D8_b$)	−14.3	−11.01 [41]		−10.6 [42]
$Co_{50}V_{50}$		−14.1	−11.26 [41]		−11.7 [42]
Co_3V	cP4 ($L1_2$)	−13.3		−16.765 [34]	
	hP24	−13.5		−17.247 [34]	
	[a] hP8 ($D0_{19}$)	−14.0			

[a] Metastable phase.

are correctly described as the most stable phases at corresponding compositions. However, the $D0_{19}$ Co_3V phase is calculated again to be slightly more stable than the equilibrium hP24 and $L1_2$ phases. According to the phase diagram [20], the hP24 with a stacking sequence of 'ABCACB' appears at lower temperature than the $L1_2$ with an 'ABC' stacking sequence. Considering again that the $D0_{19}$ has an 'AB' sequence, which is the same as pure Co, and that the difference in the calculated enthalpy of formation between the $D0_{19}$ and the other equilibrium phases is smaller than 0.01 eV, it was finally decided to accept the present interatomic potential calculation (the prediction of the $D0_{19}$ as the most stable Co_3V compound structure at 0 K).

Overall, the newly developed interatomic potentials appear to reasonably reproduce the structural and thermodynamic properties of the relevant binary systems. To further examine the quality of fitting, thermodynamic properties of liquid and FCC solution phases were also calculated. The calculated enthalpy of mixing of liquid at 1873 K and FCC random solid solution at 0 K is presented in Figs. 4 and 5, respectively, in comparison with experiments and/or CALPHAD calculations. It is shown that the present calculation is in accordance with literature data for the thermodynamic properties of solution phases in the Co–V and Co–Ti systems.

Further, the melting temperatures of Co_xTi_y and Co_xV_y compounds were also evaluated to confirm the consistency of the newly developed potentials with corresponding phase diagram information, as presented in Table 6. A small difficulty in the comparison of melting points between the present atomistic simulation and CALPHAD calculation was that most of the compounds in the phase diagrams, except the B2 CoTi, do not melt congruently but through peritectic reactions, while the present atomistic simulation for compound phases must be for the congruent melting. Consequently, Table 6 shows hypothetical metastable congruent melting points obtained from CALPHAD calculations [42,47] as well as the equilibrium peritectic temperatures on the experimentally compiled phase diagrams [18,20].

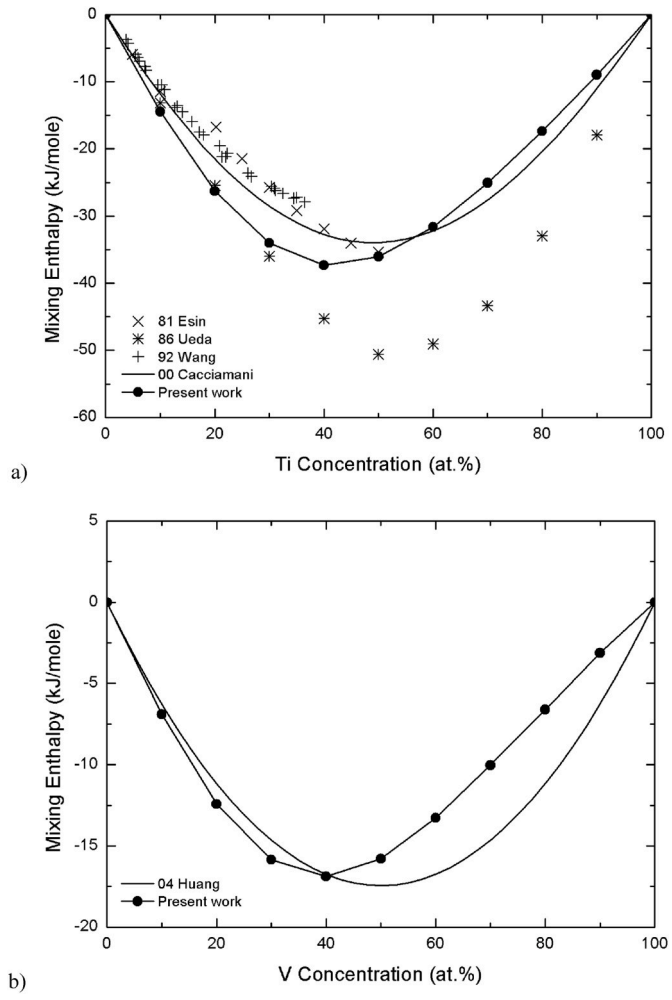

Fig. 4. Enthalpy of mixing of liquid phase for the a) Co–Ti and b) Co–V binary systems at 1873 K according to the present interatomic potentials, in comparison with experimental data [44–46] and CALPHAD assessments [42,47].

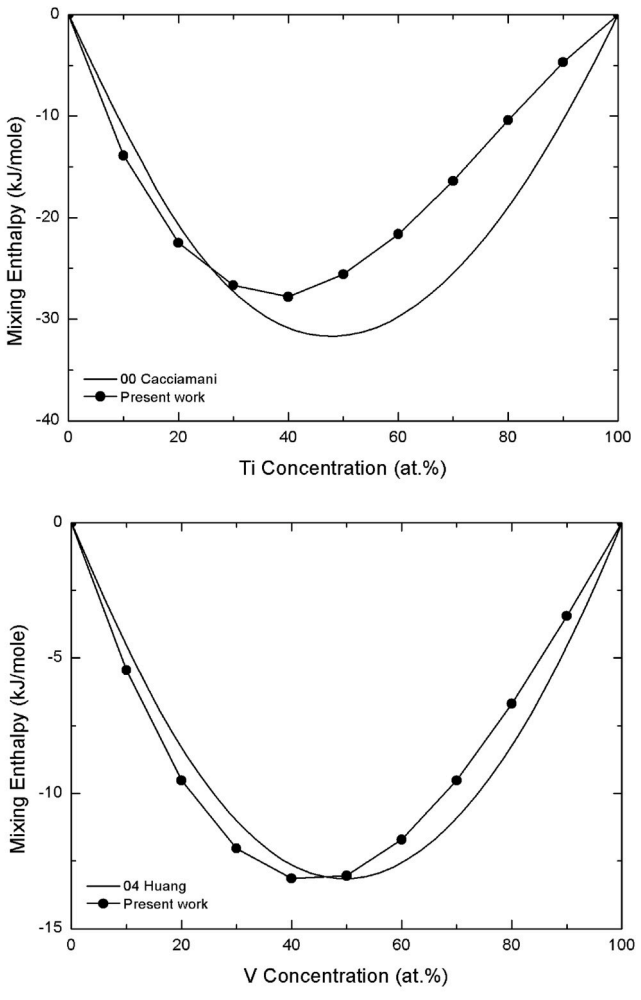

Fig. 5. Enthalpy of mixing of FCC random solid solution for the a) Co–Ti and b) Co–V binary systems at 0 K according to the present interatomic potentials, in comparison with CALPHAD assessments [42,47].

In the case of the Co–Ti system, simulated melting temperatures of pure elements and Co_xTi_y were in good agreements with literature data. It should be noted here that the present potentials cannot reproduce the hcp/fcc transformation in pure Co and the hcp/bcc transformation in pure Ti. Hcp Co and hcp Ti are the most stable structures for both elements up to melting in the present simulation. Therefore, the melting temperatures of pure Co and Ti presented in Table 6 are for hcp Co and hcp Ti, and the reference values being compared with the present simulations are metastable melting points of hcp Co and hcp Ti obtained from a CALPHAD calculation [51]. In the case of the Co–V system, it should first be noticed that the melting point of pure vanadium according to the pure V potential used in the present work is significantly lower than the experimental data. Consequently, the simulated melting points of compound phases, especially those for V-rich compounds, are lower than the corresponding reference data. Even with this incompleteness, the relative stability between the $L1_2$ Co_3V and hP24 Co_3V (the former is less stable than the latter) is correctly maintained up to the hypothetical, metastable congruent melting. The method used to calculate the melting point is the interface method [52] which, according to the present authors' experience, calculates the melting point with tens of degrees of precision. Details of the method are presented as Supplement Information.

Lastly, to confirm the robustness of the newly developed potentials at finite temperatures, the structural stability of stable compounds was checked by monitoring the structural change with increasing

Table 6
Simulated melting temperature (K) of Co, Ti, V and Co_xTi_y, Co_xV_y intermetallic compounds using the present 2NN MEAM potential, in comparison with the phase diagram and CALPHAD calculations [18,20,42,47,51].

System	Phase	Structure	Present work	Reference
Co–Ti	Co	hP2 (A3)	1642[a]	1700[a] [51]
	Ti	hP2 (A3)	1698[a]	1737[a] [51]
	$CoTi_2$	cF96 ($E9_3$)	1210[b]	1356[b] [47]
				1331[c] [18]
	CoTi	cP2 (B2)	1603	1598 [47]
	Co_2Ti	cF24 (C15)	1505[b]	1498[b] [47]
				1508[c] [18]
		hP24 (C36)	1505[b]	1494[b] [47]
				1483[c] [18]
	Co_3Ti	cP4 ($L1_2$)	1469[b]	1452[b] [47]
				1483[c] [18]
Co–V	Co	hP2 (A3)	1642[a]	1700[a] [51]
	V	cI2 (A2)	1490	2183 [51]
	CoV_3	cP8 (A15)	1445[a,b]	1714[a,b] [42]
	$Co_{40}V_{60}$	tP30 ($D8_b$)	1105	1521–1695 [20]
	Co_3V	cP4 ($L1_2$)	1306[a,b]	-
		hP24	1414[a,b]	1536[a,b] [42]

[a] Metastable melting.
[b] Hypothetical congruent melting.
[c] Peritectic reaction.

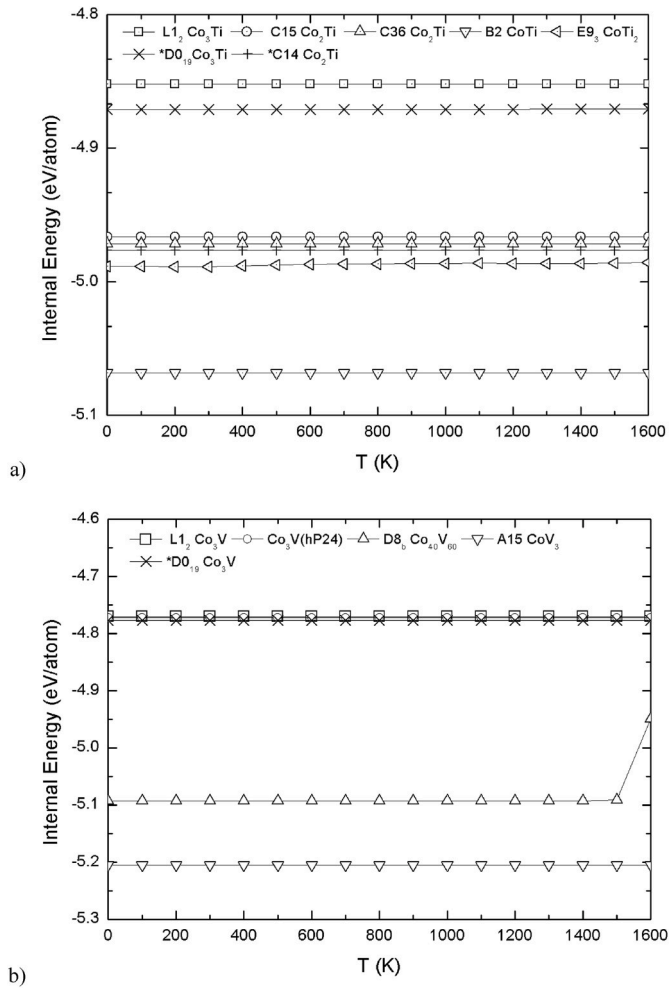

Fig. 6. Internal energy of a) Co_xTi_y and b) Co_xV_y intermetallic compounds after quenching to 0 K from the individual finite temperatures. The metastable phase is marked with an asterisk (*).

temperature. Fig. 6 shows the change in internal energy of individual Co_xTi_y and Co_xV_y compound phases after heating to each temperature and rapid cooling to 0 K. A change in the internal energy indicates a structural change. A special attention was paid to the finite temperature stability of $L1_2$ Co_3Ti and Co_3V compounds because those phases are based on the FCC structure on which most Pt, Pd-containing nano-catalysts particles are based, but are incorrectly predicted to be slightly less stable than the metastable $D0_{19}$ compounds. It is shown that all of the stable compounds (including the $L1_2$ Co_3Ti and Co_3V) maintain their original structures up to the common operating temperature of noble metal catalysts – around 1000 K.

It has been shown that the newly developed interatomic potentials for the Co–Ti and Co–V systems reproduce structural and thermodynamic properties of the relevant binary alloys in reasonable agreement with experiments, first-principles calculations, and CALPHAD-type thermodynamic assessments. It was also shown that the potentials are applicable to finite temperature simulations. In the 2NN MEAM formalism, interatomic potentials for multicomponent systems (larger than ternary) can be readily developed once only the constituent unary and binary potentials are available. The newly developed Co–Ti and Co–V potentials can be combined with the already developed Co–Fe and Co–Ni binary potentials, and also with Pt-M and Pd-M binary potentials to generate Pt–Co-M and Pd–Co-M (M = Fe, Ni, Ti, V) ternary potentials and can be utilized for atomistic simulations to design trimetallic nano-catalysts. These potentials will also be available to the public through a web-platform [48].

3. Conclusion

2NN MEAM interatomic potentials for the Co–Ti and Co–V binary systems that reasonably describe various fundamental materials properties of the relevant alloy systems are now available. The newly developed potentials can be combined with other binary potentials that were already developed to generate Pt–Co-M and Pd–Co-M ternary interatomic potentials and enable atomistic studies to investigate highly efficient Pt and Pd trimetallic nano-catalysts.

Data availability

The datasets analyzed during the current study will be made available from the corresponding author on request.

Declaration of competing interest

The authors declare that they have no known competing financial interests or personal relationships that could have appeared to influence the work reported in this paper.

Acknowledgements

This research has been financially supported by the Nano·Material Technology Development Program through the National Research Foundation of Korea (NRF) funded by the Ministry of Science and ICT (2016M3A7B4024132).

Appendix A. Supplementary data

Supplementary data to this article can be found online at https://doi.org/10.1016/j.calphad.2020.101791.

References

[1] K.D. Gilroy, A. Ruditskiy, H.-C. Peng, D. Qin, Y. Xia, Bimetallic nanocrystals: syntheses, properties, and applications, Chem. Rev. 116 (18) (2016) 10414–10472, https://doi.org/10.1021/acs.chemrev.6b00211.

[2] H. Liao, A. Fisher, Z.J. Xu, Surface segregation in bimetallic nanoparticles: a critical issue in electr^{oc}atalyst engineering, Small 11 (27) (2015) 3221–3246, https://doi.org/10.1002/smll.201403380.

[3] V.R. Stamenkovic, B.S. Mun, M. Arenz, K.J. Mayrhofer, C.A. Lucas, G. Wang, P. N. Ross, N.M. Markovic, Surface segregation in bimetallic nanoparticles: a critical issue in electrocatalyst engineering, Nat. Mater. 6 (3) (2007) 241–247, https://doi.org/10.1038/nmat1840.

[4] Z. Liu, C. Yu, I.A. Rusakova, D. Huang, P. Strasser, Synthesis of Pt_3Co alloy nanocatalyst via reverse micelle for oxygen reduction reaction in PEMFCs, Top. Catal. 49 (3) (2008) 241–250, https://doi.org/10.1007/s11244-008-9083-2.

[5] H. Li, Z. Zhu, J. Liu, S. Xie, H. Li, Hollow palladium–cobalt bimetallic nanospheres as an efficient and reusable catalyst for Sonogashira-type reactions, J. Mater. Chem. 20 (21) (2010) 4366–4370, https://doi.org/10.1039/b926347k.

[6] D. Wang, H.L. Xin, R. Hovden, H. Wang, Y. Yu, D.A. Muller, F.J. DiSalvo, H. D. Abruña, Structurally ordered intermetallic platinum–cobalt core–shell nanoparticles with enhanced activity and stability as oxygen reduction electrocatalysts, Nat. Mater. 12 (2013) 81–87, https://doi.org/10.1038/nmat3458.

[7] Y.-L. Qin, Y.-C. Liu, F. Liang, L.-M. Wang, Preparation of Pd–Co-based nanocatalysts and their superior applications in formic acid decomposition and methanol oxidation, ChemSusChem 8 (2) (2015) 260–263, https://doi.org/10.1002/cssc.201402926.

[8] L. Marks, L. Peng, J. Phys, Nanoparticle shape, thermodynamics and kinetics, Condens. Matter 28 (5) (2016), 053001, https://doi.org/10.1088/0953-8984/28/5/053001.

[9] J.-S. Kim, D. Seol, J. Ji, H.-S. Jang, Y. Kim, B.-J. Lee, Second nearest-neighbor modified embedded-atom method interatomic potentials for the Pt-M (M = Al, Co, Cu, Mo, Ni, Ti, V) binary systems, Calphad 59 (2017) 131–141, https://doi.org/10.1016/j.calphad.2017.09.005.

[10] B.-J. Lee, W.-S. Ko, H.-K. Kim, E.-H. Kim, The modified embedded-atom method interatomic potentials and recent progress in atomistic simulations, Calphad 34 (4) (2010) 510–522, https://doi.org/10.1016/j.calphad.2010.10.007.

[11] B.-J. Lee, J.-H. Shim, M.I. Baskes, Semiempirical atomic potentials for the fcc metals Cu, Ag, Au, Ni, Pd, Pt, Al, and Pb based on first and second nearest-neighbor modified embedded atom method, Phys. Rev. B 68 (14) (2003), 144112, https://doi.org/10.1103/physrevb.68.144112.

[12] G.-U. Jeong, C.S. Park, H.-S. Do, S.-M. Park, B.-J. Lee, Second nearest-neighbor modified embedded-atom method interatomic potentials for the Pd-M (M= Al, Co, Cu, Fe, Mo, Ni, Ti) binary systems, Calphad 62 (2018) 172–186, https://doi.org/10.1016/j.calphad.2018.06.006.
[13] W.-M. Choi, Y. Kim, D. Seol, B.-J. Lee, Modified embedded-atom method interatomic potentials for the Co-Cr, Co-Fe, Co-Mn, Cr-Mn and Mn-Ni binary systems, Comput. Mater. Sci. 130 (2017) 121–129, https://doi.org/10.1016/j.commatsci.2017.01.002.
[14] Y.-K. Kim, W.-S. Jung, B.-J. Lee, Modified embedded-atom method interatomic potentials for the Ni–Co binary and the Ni–Al–Co ternary systems, Model, Simul. Mat. Sci. Eng. 23 (5) (2015), 055004, https://doi.org/10.1088/0965-0393/23/5/055004.
[15] J.-S. Kim, D. Seol, B.-J. Lee, Critical assessment of Pt surface energy–An atomistic study, Surf. Sci. 670 (2018) 8–12, https://doi.org/10.1016/j.susc.2017.12.008.
[16] Y.-M. Kim, B.-J. Lee, M. Baskes, Modified embedded-atom method interatomic potentials for Ti and Zr, Phys. Rev. B 74 (1) (2006), 014101, https://doi.org/10.1103/physrevb.74.014101.
[17] B.-J. Lee, M.I. Baskes, H. Kim, Y.K. Cho, Second nearest-neighbor modified embedded atom method potentials for bcc transition metals, Phys. Rev. B 64 (18) (2001), 184102, https://doi.org/10.1103/physrevb.64.184102.
[18] J.L. Murray, The Co−Ti (Cobalt−Titanium) system, J. Phase Equil. 3 (1) (1982) 74–85, https://doi.org/10.1007/bf02873414.
[19] A. Jain*, S.P. Ong*, G. Hautier, W. Chen, W.D. Richards, S. Dacek, S. Cholia, D. Gunter, D. Skinner, G. Ceder, K.A. Persson, *=equal contributions), Commentary: the Materials Project: a materials genome approach to accelerating materials innovation, Apl. Mater. 1 (1) (2013), 011002, https://doi.org/10.1063/1.4812323.
[20] J. Smith, The Co-V (Cobalt-Vanadium) system, J. Phase Equil. 12 (3) (1991) 324–331, https://doi.org/10.1007/bf02649921.
[21] R.V. Chepulskii, S. Curtarolo, Calculation of solubility in titanium alloys from first principles, Acta Mater. 57 (18) (2009) 5314–5323, https://doi.org/10.1016/j.actamat.2009.07.037.
[22] Q. Guo, O.J. Kleppa, Standard enthalpies of formation of some alloys formed between group IV elements and group VIII elements, determined by high-temperature direct synthesis calorimetry: II. Alloys of (Ti, Zr, Hf) with (Co, Ni), J. Alloys Compd. 269 (1) (1998) 181–186, https://doi.org/10.1016/s0925-8388(98)00246-1.
[23] J. Aufrecht, W. Baumann, A. Leineweber, V. Duppel, E.j. Mittemeijer, Layer-stacking irregularities in C36-type Nb–Cr and Ti–Cr Laves phases and their relation with polytypic phase transformations, Philos. Mag. A 90 (23) (2010) 3149–3175, https://doi.org/10.1080/14786435.2010.482068.
[24] P. Duwez, J.L. Taylor, The structure of intermediate phases in alloys of titanium with iron, cobalt, and nickel, J. Occup. Med. 2 (9) (1950) 1173–1176, https://doi.org/10.1007/bf03399120.
[25] G. Purdy, R. Taggart, A substructure in omega-hardened alloys of cobalt in titanium, Trans. Am. Inst. Min. Metall. Eng. 218 (1) (1960) 186–187.
[26] Y. Aoki, K. Asami, M. Yamamoto, Transformation temperatures and magnetic properties of the ordered hexagonal VCo3 compound, Phys. Status Solidi 23 (2) (1974) K167–K169, https://doi.org/10.1002/pssa.2210230260.
[27] H. Wallbaum, H. Witte, The crystal structure of $TiCo_2$, Z. Metallkd. 31 (1939) 185–187.
[28] A. Dwight, CsCl-type equiatomic phases in binary alloys of transition elements, Trans. Am. inst. Min. Metall. Eng. 215 (2) (1959) 283–286.
[29] W.W. Xu, J.J. Han, Z.W. Wang, C.P. Wang, Y.H. Wen, X.J. Liua, Z.Z. Zhu, Thermodynamic, structural and elastic properties of Co_3X (X = Ti, Ta, W, V, Al) compounds from first-principles calculations, Intermetallics 32 (2013) 303–311, https://doi.org/10.1016/j.intermet.2012.08.022.
[30] J.-h. Xu, W. Lin, A.J. Freeman, Electronic structure and phase stability of A_3Ti (A =Fe, Co, Ni, and Cu), Phys. Rev. B 48 (7) (1993) 4276–4286, https://doi.org/10.1103/physrevb.48.4276.
[31] S. Zegler, J. Downey, Ternary Cr_3O-type phases with vanadium, Trans. Metall. AIME 227 (6) (1963) 1407.
[32] C. Paduani, C. Kuhnen, Electronic structure of A15-type compounds: V_3Co, V_3Rh, V_3Ir and V_3Os, Eur. Phys. J B 69 (3) (2009) 331–336, https://doi.org/10.1140/epjb/e2009-00181-8.
[33] H. Stuwe, Description of the sigma phase as a structure with sphere packing, Trans. Am. Inst. Min. Metall. Eng. 215 (3) (1959) 408–411.
[34] C.P. Wang, B. Deng, W.W. Xu, L.H. Yan, J.J. Han, X.J. Liu, Effects of alloying elements on relative phase stability and elastic properties of $L1_2$ Co_3V from first-principles calculations, J. Mater. Sci. 53 (2) (2018) 1204–1216, https://doi.org/10.1007/s10853-017-1549-9.
[35] S. Saito, The crystal structure of VCo_3, Acta Crystallogr. 12 (7) (1959) 500–502, https://doi.org/10.1107/s0365110x59001517.
[36] H. Yasuda, T. Takasugi, M. Koiwa, Elastic constants of Co_3Ti and CoTi intermetallic compounds, Mater. Trans., JIM 32 (1) (1991) 48–51, https://doi.org/10.2320/matertrans1989.32.48.
[37] W. Zhou, R. Sahara, K. Tsuchiya, First-principles study of the phase stability and elastic properties of Ti-X alloys (X = Mo, Nb, Al, Sn, Zr, Fe, Co, and O), J. Alloys Compd. 727 (2017) 579–595, https://doi.org/10.1016/j.jallcom.2017.08.128.
[38] A. Miedema, The formation enthalpy of monovacancies in metals and intermetallic compounds, Z. Metallkd. 70 (1979) 345–353.
[39] A. Davydov, U.R. Kattner, D. Josell, R.M. Waterstrat, W.J. Boettinger, J.E. Blendell, A.J. Shapiro, Determination of the CoTi congruent melting point and thermodynamic reassessment of the Co-Ti system, J. Metall. Mater. Trans. A 32 (9) (2001) 2175–2186, https://doi.org/10.1007/s11661-001-0193-8.
[40] P. Gomozov, Y.V. Zasypalov, B. Mogutnov, Formation enthalpies for intermetallic compounds with structure CsCl (CoTi, CoZr, CoAl, NiTi), Zh. Fiz. Khim. 60 (1986) 1865–1867.
[41] P.J. Spencer, F.H. Putland, A calorimetric study of the cobalt + vanadium system, J. Chem. Thermodyn. 8 (6) (1976) 551–556, https://doi.org/10.1016/0021-9614(76)90028-8.
[42] S. Huang, L. Li, O.V. Biest, J. Vleugels, Thermodynamic assessment of the Co–V and Co–V–C system, J. Alloys Compd. 385 (1) (2004) 114–118, https://doi.org/10.1016/j.jallcom.2004.04.131.
[43] R. Fountain, W. Forgeng, Phase relations and precipitation in Cobalt-Titanium alloys, Trans. Am. Inst. Min. Metall. Eng. 215 (6) (1959) 998–1008.
[44] H. Wang, R. Lück, B. Predel, Thermodynamic investigation of the Co-Ti system, Z. Metallkd. 83 (7) (1992) 528–532.
[45] Y. Ueda, T. Nishi, T. Oishi, K. Ono, Thermodynamic study of the liquid Ti-Co alloys by mass spectrometry, J. Japan Inst. Metals 50 (1986) 1081–1088, https://doi.org/10.2320/jinstmet1952.50.12_1081.
[46] Y. Esin, M.G. Valishev, A.F. Ermakov, P.V. Gel'd, M.S. Petrushevskii, The enthalpies of formation of liquid cobalt-titanium and tin-titanium alloys, Russ. J. Phys. Chem. 55 (3) (1981) 417–418.
[47] G. Cacciamani, R. Ferro, I. Ansara, N. Dupin, Thermodynamic modelling of the Co–Ti system, Intermetallics 8 (3) (2000) 213–222, https://doi.org/10.1016/s0966-9795(99)00098-9.
[48] qCat. http://qcat.vfab.org/.
[49] L.J. Nagel, B. Fultz, J.L. Robertson, Phase equilibria of Co_3V, J. Phase Equil. 18 (1) (1997) 21–23, https://doi.org/10.1007/BF02646756.
[50] P. Wang, T. Hammerschmidt, U.R. Kattner, G.B. Olson, Structural stability of Co–V intermetallic phases and thermodynamic description of the Co–V system, Calphad 68 (2020), 101729, https://doi.org/10.1016/j.calphad.2019.101729.
[51] A.T. Dinsdale, SGTE data for pure elements, Calphad 15 (1991) 317–425, https://doi.org/10.1016/0364-5916(91)90030-N.
[52] J.R. Morris, X. Song, The melting lines of model systems calculated from coexistence simulations, J. Chem. Phys. 116 (21) (2002) 9352–9358, https://doi.org/10.1063/1.1474581.